Title

Dynamic Effects and Hydrogen Bonding in Mixed-Halide Perovskite Solar Cell Absorbers

Journal

The Journal of Physical Chemistry Letters, 12(16)

ISSN

1948-7185

Authors

Wilks, Regan G

Erbing, Axel

Sadoughi, Golnaz

et al.

Publication Date

2021-04-29

DOI

10.1021/acs.jpclett.1c00745

Peer reviewed

Dynamic Effects and Hydrogen Bonding in Mixed-Halide Perovskite Solar Cell Absorbers

Regan G. Wilks,[1] Axel Erbing,[2] Golnaz Sadoughi,[3] David E. Starr,[1] Evelyn Handick,[1] Frank Meyer,[4] Andreas Benkert,[4,5] Marcella Iannuzzi,[6] Dirk Hauschild,[5,7,8] Wanli Yang,[9] Monika Blum,[8,9,10] Lothar Weinhardt,[5,7,8] Clemens Heske,[5,7,8] Henry J. Snaith,[3] Michael Odelius,[2*] and Marcus Bär[1,11,12]*

[1]Renewable Energy, Helmholtz-Zentrum Berlin für Materialien und Energie GmbH (HZB), Germany

[2]Department of Physics, Stockholm University, AlbaNova University Center, Stockholm, Sweden

[3]Department of Physics, Clarendon Laboratory, University of Oxford, UK

[4]Experimental Physics 7, University of Würzburg, Germany

[5]Institute for Photon Science and Synchrotron Radiation (IPS), Karlsruhe Institute of Technology (KIT), Germany

[6]Physical Chemistry Institute, University of Zürich, Zürich, Switzerland

[7]Institute for Chemical Technology and Polymer Chemistry (ITCP), Karlsruhe Institute of Technology (KIT), Germany

[8]Department of Chemistry and Biochemistry, University of Nevada, Las Vegas (UNLV), USA

[9]Advanced Light Source, Lawrence Berkeley National Laboratory, USA

[10]Chemical Sciences Division, Lawrence Berkeley National Laboratory, USA

[11]Helmholtz-Institute Erlangen-Nürnberg for Renewable Energy (HI ERN), Berlin, Germany

[12]Department of Chemistry and Pharmacy, Friedrich-Alexander-Universität Erlangen-Nürnberg (FAU), Erlangen, Germany

Corresponding Authors

Regan G. Wilks regan.wilks@helmholtz-berlin.de

Michael Odelius odelius@fysik.su.se

ABSTRACT

The organic component (methylammonium) of $CH_3NH_3PbI_{3-x}Cl_x$-based perovskite shows electronic hybridization with the inorganic framework via H-bonding between N and I sites. Femtosecond dynamics induced by core excitation are shown to strongly influence the measured x-ray emission spectra and the resonant inelastic soft x-ray scattering of the organic components. The N *K* core excitation leads to a greatly increased N-H bond length which modifies and strengthens the interaction with the inorganic framework compared to the ground state. The study indicates that excited-state dynamics must be accounted for in spectroscopic studies of this perovskite solar-cell material, and the organic-inorganic hybridization interaction suggests new avenues for probing the electronic structure of this class of materials. It is incidentally shown that beam damage to the methylamine component can be avoided by moving the sample under the soft x-ray beam to minimize exposure, and that this procedure is necessary to prevent the creation of experimental artefacts.

TOC GRAPHICS

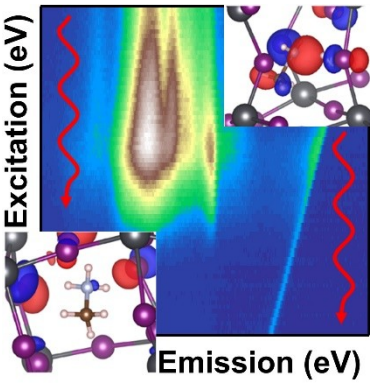

The rapid advancements in conversion efficiency of metal-halide perovskite (MHP) solar-cell devices is fueled in part by the tuneability of the material's optical and electronic properties via variation of the anion and cation constituents and ratios. The highest efficiencies are currently reached when methylammonium ($CH_3NH_3^+$, MA) is included in the cation mixture,[1,2] although it is associated with accelerated degradation of the device performance. Understanding the role of MA with respect to the electronic structure of the material and its behavior under characterization and operating conditions is needed to fully understand both the positive and negative aspects of its influence. The regions of the valence and conduction bands most associated with the optical and electronic structure are dominated by the inorganic MHP components' derived density of states – with MA seeming to play only a small role[3,4]. However, the material properties are influenced by dynamics of the organic-inorganic system on numerous time scales[2,5,6].

Combining site- and element-specific soft x-ray spectroscopic measurements of $CH_3NH_3PbI_{3-x}Cl_x$ with molecular dynamics and density functional theory modelling, we present a thorough study of the electronic structure and ultrafast dynamics of the organic MHP component. MA is related to several materials that we have previously examined using C and N *K*-edge x-ray absorption (XAS) and emission (XES) spectroscopy, as well as resonant inelastic soft x-ray

scattering (RIXS). The XES, XAS, and RIXS[7,8,9] spectra of ammonia and ammonium serve as a basis for analyzing the spectra in the MHP system. Understanding the hybridization of these groups with the carbon chain in ethylammonium (probed by XAS[10]) adds another layer of understanding. Based on previous studies of amino acids[11,12], we expect ultrafast proton dynamics in the intermediate, core-ionized state to have a strong influence on the measured spectra, and we will show that this is indeed the case in the methylammonium lead halide system. The modelling and measurement of these effects and the density of electronic states in the material describe hybridization between the organic and inorganic components of the perovskite, suggesting a new avenue for understanding the structure and dynamics of the system.

XES spectra were measured at the rollup position of beamline 8.0.1 of the Advanced Light Source, Lawrence Berkeley National Laboratory, with the high-transmission x-ray spectrometer[13] of the SALSA endstation[14]. To avoid beam-induced damage, the XES spectra were measured while the sample was moved in a direction perpendicular to the incoming photons at a speed of 400 μm/s. Given the size of the photon beam, this limits exposure of a given sample position to approximately 0.075 s. Spectra measured at lower scanning rates led to strong distortion of the spectral features, as well as the emergence of strong emission when exciting below the MA absorption onset.

Spectral modeling was accomplished based on density functional theory (DFT) using Kohn-Sham orbitals to model x-ray transitions[15]. The effects of ultrafast dynamics were included by *ab initio* molecular dynamics (AIMD) simulations of the core-ionized state. Snapshots from the AIMD trajectories at fs intervals were used to simulate individual spectra, which were then combined in a lifetime average to model the measured spectrum.

Figure 1a) compares the measured nonresonant ($h\nu_{exc}$ = 420 eV) N *K* XES spectrum of $CH_3NH_3PbI_{3-x}Cl_x$ (black dots) with the results of the spectral modeling (see Simulations section of SI for details) of $CH_3NH_3PbI_3$. (NB: There may be small differences in electronic structure between the measured $CH_3NH_3PbI_{3-x}Cl_x$ and the simulated $CH_3NH_3PbI_3$. However, it has been observed that films prepared in the described way have little or no Cl integrated into the perovskite structure[16], particularly within the near-surface interaction volume associated with XES.) Using the ground-state geometry (black line), most features in the measured spectrum can be reproduced, but there is considerable disagreement in some regions (most notably around 396 eV). When ultrafast dynamics are included in the model (red line), a more complex lineshape emerges, and it becomes clear that all features in the measured N *K* XES spectrum are represented; adding a nonuniform Lorentzian broadening (blue line, for details see the SI) to the calculation highlights the excellent agreement between measured and calculated spectra. A core-hole lifetime of 5.8 fs was used to simulate lifetime-averaged N *K* spectra, which will be described in detail when discussing Figure 2, below.

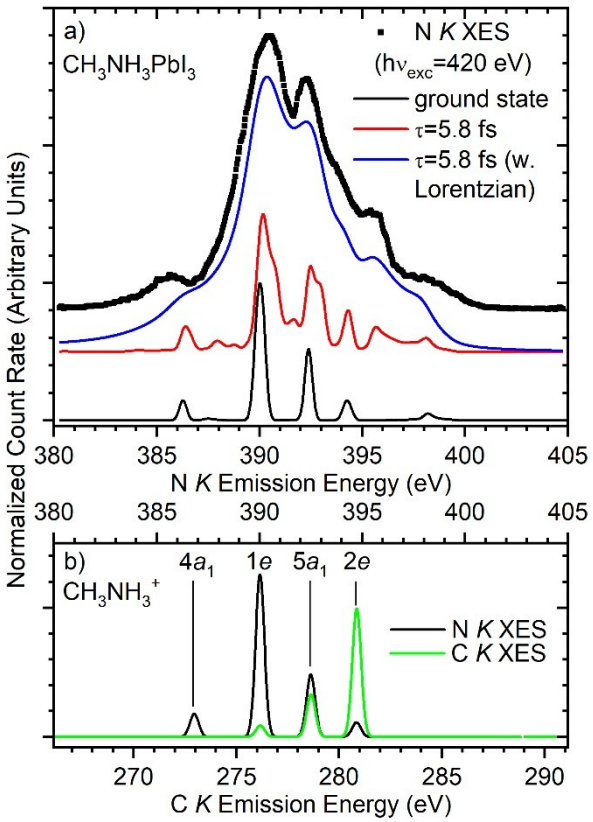

Figure 1. a) Measured N *K* XES spectrum of $CH_3NH_3PbI_{3-x}Cl_x$ (black dotted line), compared to the calculated, Gaussian-broadened $CH_3NH_3PbI_3$ spectra using the ground-state electronic structure (solid black line) and by including dynamic effects (red). A calculated spectrum with additional Lorentzian broadening (blue) is also included (on an adjusted intensity scale) for closer comparison to the measured spectrum. b) Calculated N *K* XES (black, lower abscissa) and C *K* XES (green, upper abscissa) spectra, including orbital assignment, of isolated $CH_3NH_3^+$.

For preliminary analysis of the nonresonant N *K* XES spectrum, it is useful to discuss the molecular character of the Kohn-Sham orbitals underlying the simulated spectra. As a basis, the calculated C and N *K* XES spectra of the isolated (i.e., gas-phase) MA ion – without inclusion of dynamic effects – are shown in Figure 1b, and it is clear that most features of the ground-state perovskite N *K* XES spectrum in Figure 1a are already well-represented in the gas-phase MA

spectrum. Using the notation for the C_{3v} point group symmetry of the isolated MA ion, we associate the largest peaks $1e$ and $5a_1$ with C-N bonding orbitals of π and σ symmetry, respectively. (Isodensity surfaces of the gas-phase MA orbitals are shown in Figure S1 of the supplementary information.) The $1e$ orbital has predominantly nitrogen character, and so the respective transition can contribute strongly to the N *K* XES; the corresponding anti-bonding $2e$ orbital has mainly carbon character and thus contributes only weakly. The $5a_1$ orbital is composed of atomic 2p character at both sites and contributes strongly to both N and C *K* XES. The weak $4a_1$ peak arises from a σ orbital dominated by C 2s-N 2p mixing. Altogether, this orbital analysis explains the systematic intensity differences in the N and C *K* XES spectra. Due to the localized molecular character of the corresponding orbitals (see, e.g., $2e$ in Figure 2a,iii)), the main features in the ground-state XES spectra of $CH_3NH_3PbI_3$ in Figure 1a are still dominated by the same lines as for the gas phase (isodensity surfaces of selected orbitals for $CH_3NH_3PbI_3$ are shown in Figure S2 of the supplementary information, both in ground-state and dissociated geometry).

Even in the ground state, however, distinct and important differences between MA in isolation and in the perovskite material are found. Most prominently, the feature at approximately 398 eV seen in Figure 1a has no analogue in the calculation of the gas-phase MA spectrum (Figure 1b). It is of intermolecular origin and due to the N-H···I hydrogen bond , with the underlying orbital located predominantly on iodine (as can be seen in Figure 2a,iv, discussed below). The H-bonding and other non-covalent interactions within the hybrid perovskite have been shown to play key roles in the hybrid perovskite structure[17]; here we will show that ultrafast dynamics can significantly increase and modify the contributions such interactions to the measured XES spectra.

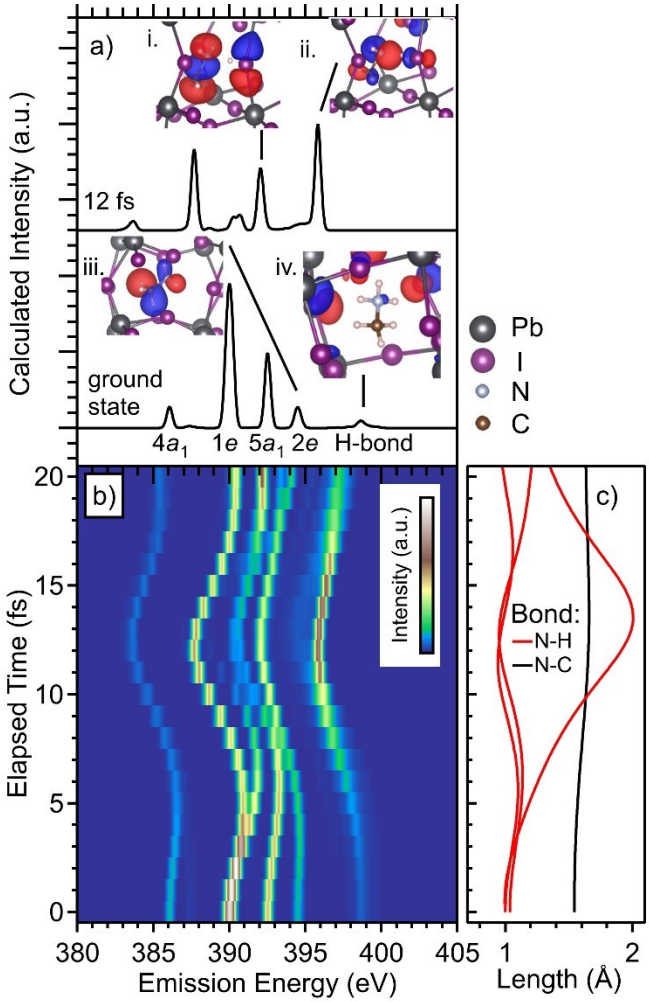

Figure 2. Simulations of the $CH_3NH_3PbI_3$ N *K* XES spectrum and its evolution as a function of elapsed time after core excitation. a) Calculated spectrum at 0 fs ("ground state", bottom) and after 12 fs of the dissociated CH_3NH_2----H^+ (top), together with exemplary orbitals (i-iv) from the two geometries. b) Calculated emission spectra, with intensity denoted by the color code, and c) N-C and N-H bond lengths as a function of time after core ionization.

The detailed effects of ultrafast dynamics on the N *K* XES spectra are shown in Figure 2b and c. Figure 2b depicts the evolution of the calculated N *K* XES spectra as the geometry of the system changes due to the perturbation created by the N 1s core ionization. The spectra (Figure 2b) and corresponding N-C and N-H bond lengths (Figure 2c) are given as a function of elapsed

time since core ionization. The modelled N *K* XES spectra in Figure 1, including dynamic effects, were created by a sum of the individual time-resolved spectra, weighted according to the exponential decay of the core-ionized state with a time constant of 5.8 fs (chosen to maximize agreement between measurement and calculation, and in good agreement with the Auger-process-dominated core-hole lifetime[18]). A similar plot of the C *K* XES, using a time constant of 8.4 fs[19], is included in Figure S3.

In the time from 0 - 12 fs after core ionization, one of the N-H bonds elongates significantly (Figure 2c). The resulting CH_3NH_2----H^+ moiety (here, we use the dashed line to denote the stretching of the N-H bond in the core-ionized state far beyond what is observed in a ground state structure) has an electronic structure that differs strongly from the intact ground state, exemplified by the calculated ground-state and 12 fs spectra and diagrams of the most relevant molecular orbitals (i-iv) in Figure 2a. Due to the substantial increase (in fact, doubling) of the N-H bond length on the time scale relevant for the XES spectra, we will denote this state as "dissociated" in the following. The strong emission at 395.4 eV is associated with a three-center N-H-I anti-bonding orbital (Figure 2a,ii) with strong N 2p - I 5p hybridization; the orbital can be seen as a hybridization of the ground-state orbitals diagrammed in Figure 2a,iii (from the $CH_3NH_3^+$ orbital 2*e*) and iv (associated with the N-H···I bond). Note that the N-H-I interaction in the core-ionized state may not strictly conform to all criteria for H-bonding[20]. Similar emission features, without strong H-bond contributions, have been modelled and measured previously: In the N *K* XES of zwitterionic glycine $NH_3^+CH_2COO^-$ [11], it emerges at a similar position due to similar femtosecond proton dynamics as described here. Somewhat analogous features are also present in the ground state of ammonia (NH_3, in both gas-phase and aqueous solution)[7] and of neutral glycine (NH_2CH_2COOH) [11].

The $5a_1$ orbital shape (Figure 2a,i) at 12 fs differs substantially from the ground state, with significant electron density on both the dissociated CH_3NH_2----H^+ moiety and the I sites. The strong hybridization that occurs upon creation of the core hole suggests that, despite the small degree of interaction between the MA and the inorganic framework in the ground state of $CH_3NH_3PbI_3$, N *K* XES can probe the valence electronic structure of the material via the interactions that arise due to ultrafast dynamics.

The ultrafast production of the dissociated CH_3NH_2----H^+ moiety indicates that deprotonation of the ammonium site can occur even for the smallest photon flux, as such ultrafast processes are inherent to the measurement technique. They thus are very different from beam damage due to secondary processes (e.g., emission of Auger electrons with a two-hole final state), which can be minimized by reducing the x-ray dose to a given sample volume. The observed deprotonation of the ammonium group could trigger reactions leading to degradation of the perovskite. For example, it has previously been reported by Kerner *et al.*[22,23] that an amine group, such as that in deprotonated $CH_3NH_3^+$, can react with a PbI_2 impurity to form a Pb-alkylamide CH_3NHPbI (NB: the complete reaction requires two CH_2NH_2 and two PbI_2 to form a $CH_3NH_3PbI_3$ perovskite and the Pb-alkylamide). Kerner *et al.* find that CH_3NHPbI impurities in halide perovskites can degrade with moderate energy input (i.e., by ambient visible light, not only by x-rays) and without the need for additional reagents to form Pb^0 impurities under illumination[23]. The requirement for excess PbI_2 (which may or may not be present in the material, depending on the specific synthesis conditions) to induce Pb^0 impurities is consistent with a previous report of photoinduced production of such impurities in mixed-ion $(CH_2(NH_2)_2PbI_3)_{0.85}(CH_2NH_3PbBr_3)_{0.15}$ perovskites with slight PbI_2 excess, even when x-ray exposure is kept to minimal levels to prevent beam damage[24]. Several pathways for producing Pb^0 are proposed in[23] and elsewhere[24-27],

some of which lead to the release of iodine, which has been shown to aggressively degrade these materials, possibly leading to the fast production of other impurities within the sample. The Pb-alkylamide, with its singly-protonated N site, is a candidate for the impurity species giving rise to the pre-edge absorption resonance at 399.9 eV in the current study (see Figure S4). The expected strong pre-edge feature in the N *K*-edge XAS of such a compound[28] suggests that its contribution would be minimal when exciting across the main resonance of the sample. We have previously observed Pb^0 impurities in similar samples to those studied here[29].

To further investigate the electronic structure of $CH_3NH_3PbI_{3-x}Cl_x$, RIXS measurements at the N *K* edge are shown in Figure 3. As a function of excitation energy, we find strong variations in absolute and relative intensities of the different spectral features. Figure 3a shows three spectra, extracted from the RIXS map in Figure 3c, resonantly excited at three distinct energies: 404.0 eV (the first resonance), 405.5 eV (the maximum of the main resonance), and 408.8 eV (above the resonances; note the similar shape to the nonresonantly excited spectrum in Figure 1). For on-resonance excitation, particularly into the first resonance, the shape of the spectrum differs significantly from the nonresonant spectrum (Figure 1). The intensity of the 395.4 eV peak is strongly enhanced under core excitation (compared to core *ionization*), and an overall broadening toward lower emission energies appears in the main emission features. Comparison with the time-resolved models in Figure 2 suggests that these effects are consistent with an increased contribution from the dissociated CH_3NH_2----H^+ moiety (i.e., the positions of $5a_1$ and $1e$ orbitals in the spectra around 12 fs match, respectively, the increased intensity observed around 388 eV and 392 eV in the resonantly core-excited spectra). However, the resonant spectra cannot be simply explained by an increased excited state lifetime, as the 404.0 eV-excited spectrum does not resemble the calculated spectra with larger time constants (shown in Figure

S5). The effect is therefore rather due to changes in the local potential of the core-excited state compared to the ionized state, and/or to changes in the fluorescence cross section under resonant excitation.

The characteristics of the Rayleigh line, which appears as a diagonal line in Figure 3c, also differ on- and off-resonance, with a strong increase in both relative and absolute intensity in the region between 404 and 406 eV, indicating core-excitonic effects[30]. The differing character of the Rayleigh line (participator emission) and main fluorescence (spectator emission) intensity is shown by the partial fluorescence yield (PFY) spectra in Figure 3d, which tracks the respective normalized emission intensity as a function of excitation energy. NB: the intensity normalization is chosen to accentuate the common onset energy of the two absorption spectra and their differing lineshapes, rather than to quantify the intensity changes. In this region, the Rayleigh line also becomes strongly asymmetric toward lower emission energies. The change in lineshape is illustrated in Figure 3b, where three representative Rayleigh lines from below- (398.0 eV), above-, and on-resonance are plotted on an energy-loss scale. An average of all the Rayleigh lines from the region 404.4 - 406.0 eV, corresponding to the core-excitonic region discussed above, is also included to show the modification in lineshape with improved statistics. In the resonant region, the Rayleigh line shows energy loss features associated with vibrational final states, two of which are labelled V_1 and V_2 in Figure 3b;the vibrational structure is presumably related to the N-H bond elongation, but would require higher-resolution experimental data and appropriate modeling to describe further. The additional low-energy broadening is likely due to a combination of further vibrational-excited states and a dissociation (or varying H-bonding) attributed to proton dynamics[7,31]. These effects are consistent with the discussion of the changes in spectator emission in Figure 3a and c discussed above. Above resonance (408.8 eV), these

energy losses contribute only a slight broadening of the Rayleigh line, which can be seen when comparing to the 398 eV (below-resonance) line.

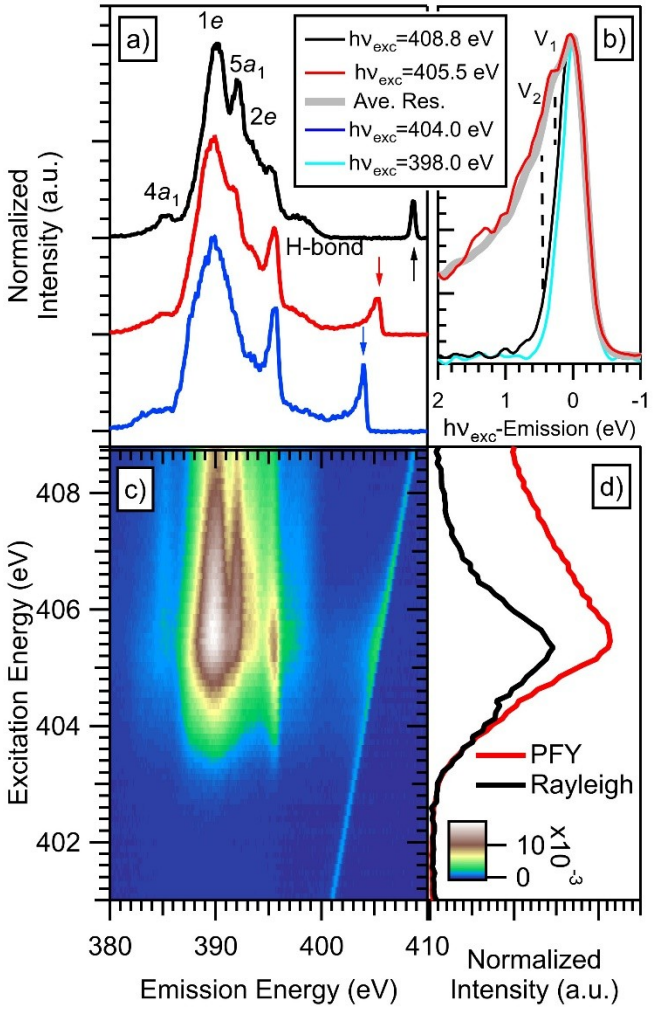

Figure 3. N *K*-edge RIXS analysis of $CH_3NH_3PbI_{3-x}Cl_x$. a) Selected emission spectra, excited above the main absorption resonance (408.8 eV), at the maximum of the main resonance (405.5 eV), and on the first resonance (404.0 eV). Spectra are normalized to the main resonance and vertically stacked for clarity. Rayleigh lines are indicated by arrows. b) Rayleigh lines excited above resonance, at the maximum of the main resonance, and well below the absorption onset (398.0 eV), shown on an energy-loss scale. The average of the Rayleigh lines in the resonance region (404.4 eV – 406.0 eV) is also included (thick gray line). Intensities are normalized to the

peak maximum. c) N *K*-edge RIXS map of $CH_3NH_3PbI_{3-x}Cl_x$, color code indicates spectral intensity. Spectra in a) and b) are extracted from this map. d) Absorption spectra, showing integral intensity from the entire RIXS map region (PFY, red) and the Rayleigh line only (black). A uniform background signal was subtracted from both, and their intensities were normalized to overlap at the absorption onset.

In summary, ultrafast proton dynamics thus play a significant part in forming the N *K* XES spectrum of $CH_3NH_3PbI_{3-x}Cl_x$, and to a much lesser extent in the corresponding C *K* XES, as shown by comparing measured and simulated spectra based on molecular dynamics and density functional theory. The primary effect is an elongation of a N-H bond, forming a dissociated CH_3NH_2----H^+ moiety characterized by a three-center N-H-I orbital. The electronic structure calculations indicate a hybridization between the organic cation and the highest occupied orbital of the system, which is located on the anion. This hybridization is present, but weak, in the ground-state geometry of the system, while it is strongly enhanced in the excited state. This suggests an interesting opportunity for future research, as XES of the organic cation can now be used to probe the electronic structure *of the anion* as well.

ACKNOWLEDGMENT

M.O. acknowledges financial support obtained from the Swedish Energy Agency (contract 2017-006797), the Carl Tryggers Foundation (contract CTS18:285), and the Swedish Research Council (VR contracts 2016-04590 and 2020-03369). The calculations were performed on resources provided by the Swedish National Infrastructure for Computing (SNIC). This research

used resources of the Advanced Light Source, which is a U.S. Department of Energy (DOE) Office of Science User Facility under Contract No. DE-AC02-05CH11231. GS and HJS received funding from the Engineering and Physical Science Research Council, UK.

REFERENCES

1 J.J. Yoo, S. Wieghold, M.C. Sponseller, M.R. Chua, S.N. Bertram, N.T.P. Hartono, J.S. Tresback, E.C. Hansen, J.-Pablo Correa-Baena, V. Bulović; *et al.* "An Interface Stabilized Perovskite Solar Cell with High Stabilized Efficiency and Low Voltage Loss" *Energy Environ. Sci.* **2019**, *12*, 2192.

2 G. Fisicaro, A. La Magna, A. Alberti, E. Smecca, G. Mannino, and I. Deretzis, "Local Order and Rotational Dynamics in Mixed A-Cation Lead Iodide Perovskites" *J. Phys. Chem. Lett.* **2020**, *11* (3), 1068-1074.

3 B. Philippe, T.J. Jacobsson, J.-P. Correa-Baena, N.K. Jena, A. Banerjee, S. Chakraborty, U.B. Cappel, R. Ahuja, A. Hagfeldt, M. Odelius; *et al.* "Valence Level Character in a Mixed Perovskite Material and Determination of the Valence Band Maximum from Photoelectron Spectroscopy: Variation with Photon Energy" *J. Phys. Chem. C* **2017**, *121* (48), 26655-26666.

4 C. Vorwerk, C. Hartmann, C. Cocchi, G. Sadoughi, S.N. Habisreutinger, R. Félix, R.G. Wilks, H.J. Snaith, M. Bär, and C. Draxl, "Exciton-Dominated Core-Level Absorption Spectra of Hybrid Organic–Inorganic Lead Halide Perovskites" *J.Phys. Chem. Lett.* **2018**, *9* (8), 1852-1858.

5 L.M. Herz, "How Lattice Dynamics Moderate the Electronic Properties of Metal-Halide Perovskites" *J. Phys. Chem. Lett.* **2018**, *9* (23), 6853-6863.

6 D.A. Egger, A.M. Rappe, and L. Kronik, "Hybrid Organic–Inorganic Perovskites on the Move" *Acc. Chem. Res.* **2016**, *49* (3), 573-581.

7 L. Weinhardt, E. Ertan, M. Iannuzzi, M. Weigand, O. Fuchs, M. Bär, M. Blum, J. D. Denlinger, W. Yang, E. Umbach; *et al.* "Probing Hydrogen Bonding Orbitals: Resonant Inelastic Soft X-ray Scattering of Aqueous NH_3" *Phys. Chem. Chem. Phys.* **2015**, *17*, 27145.

8 M. Ekimova, W. Quevedo, Ł. Szyc, M. Iannuzzi, P. Wernet, M. Odelius, and Erik T. J. Nibbering, "Aqueous Solvation of Ammonia and Ammonium: Probing Hydrogen Bond Motifs with FT-IR and Soft X-ray Spectroscopy" *J. Am. Chem. Soc.* **2017**, *139*, 12773−12783.

9 L. Weinhardt, M. Weigand, O. Fuchs, M. Bär, M. Blum, J. D. Denlinger, W. Yang, E. Umbach, and C. Heske, "Nuclear Dynamics in the Core-Excited State of Aqueous Ammonia Probed by Resonant Inelastic Soft X-ray Scattering" *Phys. Rev. B* **2011**, *84*, 104202.

10 M. Ekimova, M. Kubin, M. Ochmann, J. Ludwig, N. Huse, P. Wernet, M. Odelius, and E.T.J. Nibbering, "Soft X-ray Spectroscopy of the Amine Group: Hydrogen Bond Motifs in Alkylamine/Alkylammonium Acid−Base Pairs" *J. Phys. Chem. B* **2018**, *122*, 7737−7746.

11 M. Blum, M. Odelius, L. Weinhardt, S. Pookpanratana, M. Bär, Y. Zhang, O. Fuchs, W. Yang, E. Umbach, and C. Heske, "Ultrafast Proton Dynamics in Aqueous Amino Acid Solutions Studied by Resonant Inelastic Soft X-ray Scattering" *J. Phys. Chem. B* **2012**, *116*, 13757−13764.

12 F. Meyer, M. Blum, A. Benkert, D. Hauschild, S. Nagarajan, R. G. Wilks, J. Andersson, W. Yang, M. Zharnikov, M. Bär; *et al.* "X-ray Emission Spectroscopy of Proteinogenic Amino Acids at All Relevant Absorption Edges" *J. Phys. Chem. B* **2014**, *118*, 13142−13150.

13 O. Fuchs, M. Blum, M. Weigand, E. Umbach, L. Weinhardt, M. Bär, C. Heske, J.D. Denlinger, Y.-D. Chuang, W. McKinney; *et al.* "High-resolution, high-transmission soft x-ray spectrometer for the study of biological samples" *Rev. Sci. Instrum.* **2009**, *80*, 063103-1-7.

14 M. Blum, L. Weinhardt, O. Fuchs, M. Bär, Y. Zhang, M. Weigand, S. Krause, S. Pookpanratana, T. Hofmann, W. Yang; *et al.* "Solid And Liquid Spectroscopic Analysis (SALSA) -- a Soft X-ray Spectroscopy Endstation with a Novel Flow-Through Liquid Cell" *Rev. Sci. Instrum.* **2009**, *80*, 123102-1-6.

15 M. Iannuzzi and J. Hutter, "Inner-Shell Spectroscopy by the Gaussian and Augmented Plane Wave Method" *Phys. Chem. Chem. Phys.* **2007**, *9*, 1599.

16 D.E. Starr, G. Sadoughi, E. Handick, R.G. Wilks, J.-H. Alsmeier, L. Köhler, M. Gorgoi, H. Snaith and M. Bär, "Direct Observation of an Inhomogeneous Chlorine

Distribution in $CH_3NH_3PbI_{3-x}Cl_x$ Layers: Surface Depletion and Interface Enrichment" *Energy Environ. Sci.* **2015**, *8*, 1609.

17 P.R. Varadwaj, A. Varadwaj, H.M. Marques, and K. Yamashita, "Significance of Hydrogen Bonding and other Noncovalent Interactions in Determining Octahedral Tilting in the $CH_3NH_3PbI_3$ Hybrid Organic-Inorganic Halide Perovskite Solar Cell Semiconductor" *Sci. Rep*. **2019**, *9*, 50.

18 B. Kempgens, A. Kivimäki, M. Neeb, H.M. Köppe, A.M. Bradshaw, and J. Feldhaus, "A High-Resolution N 1s Photoionization Study of the N_2 Molecule in the Near-Threshold Region" *J. Phys. B: At. Mol. Opt. Phys.* **1996**, *29*, 2389-5402.

19 H.M. Köppe, A.L.D. Kilcoyne, J. Feldhaus, and A.M. Bradshaw, "Relaxation Effects in C 1s Photoionisation of CO: A High Resolution Photoelectron Study in the Near-Threshold Region" *J. Electron Spectrosc.* **1995**, *75*, 97-108.

20 E. Arunan, G.R. Desiraju, R.A. Klein, J. Sadlej, S. Scheiner, I. Alkorta, D.C. Clary, R.H. Crabtree, J.J. Dannenberg, P. Hobza; *et al.* "Definition of the Hydrogen Bond (IUPAC Recommendations 2011)" *Pure Appl. Chem.*, **2011**, *83*, 1637-1641.

21 M.-C. Jung, Y.M. Lee, H.-K. Lee, J. Park, S.R. Raga, L.K. Ono, S. Wang, M.R. Leyden, B.D. Yu, S. Hong; *et al.* "The Presence of CH_3NH_2 Neutral Species in Organometal Halide Perovskite Films" *Appl. Phys. Lett.* **2016**, *108*, 073901.

22 R.A. Kerner, T.H. Schloemer, P. Schulz, J.J. Berry, J. Schwartz, A. Sellinger, and B.P. Rand, "Amine Additive Reactions Induced by the Soft Lewis Acidity of Pb^{2+}

in Halide Perovskites. Part I: Evidence for Pb–Alkylamide Formation" *J. Mater. Chem. C*, **2019**, *7*, 5251-5259.

23 R.A. Kerner, T.H. Schloemer, P. Schulz, J.J. Berry, J. Schwartz, A. Sellinger, and B.P. Rand, "Amine Additive Reactions Induced by the Soft Lewis Acidity of Pb^{2+} in Halide Perovskites. Part II: Impacts of Amido Pb Impurities in Methylammonium Lead Triiodide Thin Films" *J. Mater. Chem. C*, **2019**, *7*, 5244-5250.

24 U.B. Cappel, S. Svanström, V. Lanzilotto, F.O.L. Johansson, K. Aitola, B. Philippe, E. Giangrisostomi, R. Ovsyannikov, T. Leitner, A. Föhlisch; *et al.* "Partially Reversible Photoinduced Chemical Changes in a Mixed-Ion Perovskite Material for Solar Cells" *ACS Appl. Mater. Interf.* **2017**, *9*, 34970-34978.

25 K.X. Steirer, P. Schulz, G. Teeter, V. Stevanovic, M. Yang, K. Zhu, and J. J. Berry, "Defect Tolerance in Methylammonium Lead Triiodide Perovskite" *ACS Energy Lett.*, **2016**, *1*, 360–366.

26 F.-S. Zu, P. Amsalem, I. Salzmann, R.-B. Wang, M. Ralaiarisoa, S. Kowarik, S. Duhm, and N. Koch, "Impact of White Light Illumination on the Electronic and Chemical Structures of Mixed Halide and Single Crystal Perovskites" *Adv. Opt. Mater.*, **2017**, *5*, 1700139.

27 Y. Li, X. Xu, C. Wang, B. Ecker, J. Yang, J. Huang, and Y. Gao, "Light-Induced Degradation of $CH_3NH_3PbI_3$ Hybrid Perovskite Thin Film" *J. Phys. Chem. C*, **2017**, *121*, 3904–3910.

28 R.G. Wilks, J.B. MacNaughton, H.-B. Kraatz, T. Regier, R.I.R. Blyth, and A. Moewes, "A Comparative Theoretical and Experimental Study of the Radiation Induced Decomposition of Glycine" *J. Phys. Chem. A* **2009**, *113*, 5360.

29 G. Sadoughi, D.E. Starr, E. Handick, S. Stranks, M. Gorgoi, R.G. Wilks, M. Bär, and H. Snaith, "Observation and Mediation of the Presence of Metallic Lead in Organic-Inorganic Perovskite Films" *ACS Appl. Mater. Interf.* **2015**, *7*, 13440.

30 L. Weinhardt, O. Fuchs, D. Batchelor, M. Bär, M. Blum, J. D. Denlinger, W. Yang, A. Schöll, F. Reinert, E. Umbach; *et al.* "Electron-Hole Correlation Effects in Core Level Spectroscopy Probed by the Resonant Inelastic Soft X-ray Scattering Map of C_{60}" *J. Chem. Phys.* **2011**, *135*, 104705.

31 V. Vaz da Cruz, F. Gel'mukhanov, S. Eckert, M. Iannuzzi, E. Ertan, A. Pietzsch, R.C. Couto, J. Niskanen, M. Fondell, M. Dantz, T. Schmitt, X. Lu, D. McNally, R.M. Jay, V. Kimberg, A. Föhlisch, and M. Odelius "Probing hydrogen bond strength in liquid water by resonant inelastic X-ray scattering" *Nat. Commun.* **2019**, *10***,** 1013.

32 S. Wang, Y. Jiang, E.J. Juarez-Perez, L.K. Ono, and Y. Qi, "Accelerated Degradation of Methylammonium Lead Iodide Perovskites Induced by Exposure to Iodine Vapour" *Nature Energy* **2016**, *2*, 16195.

33 R.G. Wilks and M. Bär, "Danger From Within" *Nature Energy* **2017**, *2*, 16204/1-2.

34 M.M. Lee, J. Teuscher, T. Miyasaka, T.N. Murakami, and H.J. Snaith, "Efficient Hybrid Solar Cells Based on Meso-Superstructured Organometal Halide Perovskites" *Science* **2012**, *338*, 643.